

## ***Supplementary Information***

### **Unexpected electron spin density on the axial methionine ligand in Cu<sub>A</sub> suggests its involvement in electron pathways**

Marcos N. Morgada,<sup>1,2\*</sup> María-Eugenia Llases,<sup>1\*</sup> Estefania Giannini,<sup>1</sup> Maria-Ana Castro,<sup>3</sup> Pedro M. Alzari,<sup>4</sup>  
Daniel H. Murgida,<sup>4</sup> María-Natalia Lisa<sup>1,5</sup> and Alejandro J. Vila<sup>1,2,5#</sup>

<sup>1</sup> Instituto de Biología Molecular y Celular de Rosario (IBR, CONICET-UNR), Ocampo y Esmeralda, Rosario 2000, Argentina

<sup>2</sup> Área Biofísica, Departamento de Química Biológica, Facultad de Ciencias Bioquímicas y Farmacéuticas, Universidad Nacional de Rosario, Suipacha 531, Rosario 2000, Argentina

<sup>3</sup> Instituto de Química Física de los Materiales, Medio Ambiente y Energía (INQUIMAE), Departamento de Química Inorgánica, Analítica y Química Física, Facultad de Ciencias Exactas y Naturales, Universidad de Buenos Aires and CONICET, Buenos Aires 1428, Argentina

<sup>4</sup> Institut Pasteur, Unité de Microbiologie Structurale, CNRS UMR 3528 - Université Paris Diderot, Paris 75015, France

<sup>5</sup> Plataforma de Biología Estructural y Metabolómica (PLABEM), Ocampo y Esmeralda, Rosario 2000, Argentina

\*MEL and MNM contributed equally to this paper.

#To whom correspondence should be addressed (vila@ibr-conicet.gov.ar)

## Materials and Methods

Chemicals were purchased from Sigma-Aldrich otherwise stated.  $^{13}\text{C}$ -labeled Met and  $\epsilon$ - $^{13}\text{CH}_3$  labeled Met were purchased from Cortecnet.

### *Protein expression and purification*

Selectively labeled samples on the Met residues were obtained by overexpression in *E. coli* cells by addition of the corresponding labeled Met after induction with IPTG and expression for 4 h at 37°C or overnight at 30°C. Cells then were harvested and the proteins were purified following previously optimized protocols.<sup>1,2</sup>

For crystallization, *Tt3Lh* variant was purified with an N-terminal His<sub>6</sub> tag using a His-Trap column (GE Healthcare). The tag was then cleaved with Thrombin protease (Sigma) for 12 h followed by size exclusion chromatography to remove the protease and the Tag.

### *Protein NMR spectroscopy*

NMR experiments were carried out on a Bruker Avance II Spectrometer operating at 600.13 MHz (1H frequency).  $^1\text{H}$  and  $^1\text{H}$ - $^{13}\text{C}$  HMQC/HSQC spectra were acquired with a triple-resonance (TXI) probehead and direct  $^{13}\text{C}$  acquisition NMR spectra were acquired with a broadband observe (BBO) probehead tuned at the proper frequency.

1D  $^1\text{H}$  spectra were acquired with spectral windows of 48 to 360 kHz using presaturation, PASE and SuperWEFT schemes (total recycle times around 100 ms and 10 ms for H<sub>2</sub>O and D<sub>2</sub>O samples, respectively). 2D  $^1\text{H}$ - $^1\text{H}$  NOESY spectrum were acquired using a phase-sensitive NOESY sequence with solvent presaturation in 99.9% D<sub>2</sub>O samples. The spectral window was set to 36 kHz and mixing times ranged between 4 to 20 ms.  $^1\text{H}$ ,  $^{13}\text{C}$  HMQC experiments were acquired on spectral widths ranging from 48 to 360 kHz in the  $^1\text{H}$  dimension (1024 points) and 36 to 100 kHz in the indirect dimension (32 points). The delay for coherence transfer was set to 2 ms, and the relaxation delay was set to 30 ms.  $^1\text{H}$ ,  $^{13}\text{C}$  HMQC experiments on  $\epsilon$ - $^{13}\text{CH}_3$  Met samples were acquired using a spectral window of 6 kHz in the direct dimension and 12 kHz in the indirect dimension. The delay for magnetization coherence transfer was set to 1.67 ms, optimized for the detection of the paramagnetic signal.

1D  $^{13}\text{C}$  NMR spectra were acquired using an excitation pulse of 6.9  $\mu\text{s}$  at 12.6 W using inverse-gated decoupling. The carrier frequency was set to 800, 200, or -450 ppm depending on the group of signals being studied. Spectral window and delays also varied in each experiment, which resulted in total recycle times of approximately 20 ms for the acquisition of signals around 1000 and -450 ppm, and approximately 100 ms for those near the diamagnetic region. No further signals were detected when the carrier was moved to different frequency offsets.

Signal assignment of the spectra of *Tt3LAt* was done based on a set of different homonuclear and heteronuclear spectra. Intra-residual signal connectivities were made by  $^1\text{H}$ - $^1\text{H}$  NOESY experiments in 10% and 99.9% D<sub>2</sub>O with mixing times between 4 and 20 ms.  $^{13}\text{C}$  signals were assigned by means of  $^1\text{H}$ ,  $^{13}\text{C}$  HMQC spectra tailored to the paramagnetic nature of the resonances, as already reported.

Analyses of the chemical shifts and their temperature dependences were performed as described previously.<sup>2-5</sup>

### **Determination of contact shifts**

The contact contributions ( $\delta_{con}$ ) to the chemical shifts (Tables 1 and S3) were calculated from:

$$\delta_{con} = \delta_{obs} - \delta_{dia} - \delta_{pc} \quad (1)$$

Diamagnetic chemical shifts ( $\delta_{dia}$ ) were obtained by saturation transfer difference experiments in samples containing ~10% reduced protein, by addition of substoichiometric amounts of sodium ascorbate to the fully oxidized sample. Signals were irradiated for ~50 ms at a power of ~5 mW.

Pseudocontact shifts ( $\delta_{pc}$ ) were estimated using:

$$\delta_{pc} = \frac{\mu_0 \mu_B^2 S(S+1)}{4\pi 9k_B T r^3} (3\cos^2\theta - 1)(g_{\parallel}^2 - g_{\perp}^2) \quad (2)$$

where  $\mu_0$  is the vacuum permeability,  $\mu_B$  is the Bohr magneton,  $S$  is the electronic spin (1/2 for the oxidized  $\text{Cu}_A$  center),  $k_B$  is Boltzmann's constant,  $T$  is the temperature in Kelvin,  $r$  is the module of a vector  $r$  connecting the nucleus and the averaged coordinates of both copper ions,  $\theta$  is the angle between the  $z$  component of the  $g$  tensor and the  $r$  vector, and  $g_{\parallel}$  and  $g_{\perp}$  are the parallel and perpendicular values of the axial  $g$  tensor. Distances and angles were obtained from the corresponding crystal structures.  $g_{\parallel}$  and  $g_{\perp}$  were obtained from the EPR spectra of each protein in X band (frequency = 9.4 MHz), 4K (data not shown). This approach is valid for systems with null or small spin-orbit coupling, such as the present one. Magnetic axes were defined as described by Neese and co-workers.<sup>6</sup> The pseudocontact shift proved to be small in all cases (Table S3), as expected.

### **Protein crystallization, data collection and structure determination**

Crystallization screenings were carried out using the sitting-drop vapor diffusion method and a Gryphon (Art Robbins Instruments) or a Mosquito (TTP Labtech) nanoliter-dispensing crystallization robot. Crystals of *hTt3L* grew after 1 day from an 80 mg/ml protein solution, by mixing equal volumes of protein solution and mother liquor (100 mM Hepes, 1.6 M  $(\text{NH}_4)_2\text{SO}_4$ , 0.1 mM NaCl, pH 7.5), at 18 °C. Similarly, crystals of *Tt3LAT* grew after 3 days from a 75 mg/ml protein solution, using 100 mM Hepes, 1.5 M  $\text{LiSO}_4$ , pH 7.5, as mother liquor. In both cases, single crystals were cryoprotected in mother liquor containing 30% glycerol as cryoprotectant and flash-frozen in liquid nitrogen. X-ray diffraction data were collected at the synchrotron beamline ID23-1 (ESRF, Grenoble, France), at 100 K, using wavelengths of 1.367875 Å and 1.382671 Å (to confirm the presence and location of the copper ions). Diffraction data were processed using XDS<sup>3</sup> and scaled with Aimless<sup>7</sup> from the CCP4 program suite.<sup>8</sup>

The crystal structures of *Tt3Lh* and *Tt3LAT* were solved by molecular replacement using the program Phaser<sup>9</sup> and the atomic coordinates of the soluble subunit II from Cytochrome *c* oxidase from *Thermus thermophilus* (PDB ID code 2CUA, chain A) as search probe<sup>10</sup>. The structures were refined by iterative cycles of manual model building with Coot<sup>11</sup> and refinement with Phenix.refine<sup>12,13</sup>. Copper atoms were

manually placed in  $mF_o-DF_c$  sigma-A-weighted electron density maps employing COOT and the resulting models were refined as described above. The final structures were validated through the Molprobity server (<http://molprobity.biochem.duke.edu>)<sup>14</sup>. They contained more than 97% of residues within favored regions of the Ramachandran plot, with no outliers. Figures were generated and rendered with Pymol version 2.0 (Schrödinger, LLC). Atomic coordinates and structure factors were deposited in the Protein Data Bank under the accession codes 6PTY (*Tt3Lh*) and 6PTT (*Tt3LAt*).

### ***Computational methods***

The initial structure of oxidized *Tt* Cu<sub>A</sub> was obtained from PDB ID code 2CUA and was relaxed through an equilibration process which consisted of an energy minimization followed by a slow heating from 0 K to 300K (400 ps). Starting from these equilibrated structures, 20 ns long production MD simulations in explicit water were performed at 1 atm and 300 K using the Berendsen barostat and thermostat, respectively. Periodic boundary conditions and Ewald sums were used to treat long-range electrostatic interactions and a 12 Å cut-off was used for computing direct interactions. In order to keep bonds involving hydrogen atoms at their equilibrium length, the SHAKE algorithm was used. All simulations were performed with the PMEMD module of the AMBER16 package<sup>15-17</sup>. The Amber ff14SB force field was used for all residues but the Cu site, whose parameters were developed using the MCPB.py model in AmberTools17<sup>18</sup>. Snapshots of each system were slowly cooled to 0 K (200 ps) in order to obtain the initial structures for the QM/MM simulations. These were performed at the DFT level using the SIESTA<sup>19</sup> code with the QM/MM implementation Hybrid<sup>20</sup>. For all atoms, basis sets of double zeta plus polarization quality were employed with cut-off and energy shift values of 150 Ry and 25 meV. All calculations were performed under the spin-unrestricted approximation using the generalized gradient approximation functional proposed by Perdew, Burke, and Ernzerhof (PBE)<sup>21</sup>. The scaled position link atom method was used to treat the interface between the QM and MM sections. Due to the fact that the carbonyl ligand is involved in a backbone amide bond, a large QM subsystem was required in order to assure stability. This QM section included both copper atoms and the aminoacids shown in Table S1. The rest of the protein and water molecules were treated classically using the Amber force field. All atoms included in the MD simulation were included in the QM/MM system and geometry optimization was performed at the QM/MM level for both proteins. Finally, single point QM calculations at the DFT level were performed on the optimized QM section using Gaussian09<sup>22</sup> in order to obtain spin densities. The mixed triple-zeta/double zeta (TZVP) basis set was used for Cu and S atoms, while the 6-31G\* basis set were used on all the other atoms. Atom contributions to molecular orbitals were computed with the software Chemissian.

SUPPLEMENTARY FIGURES AND TABLES

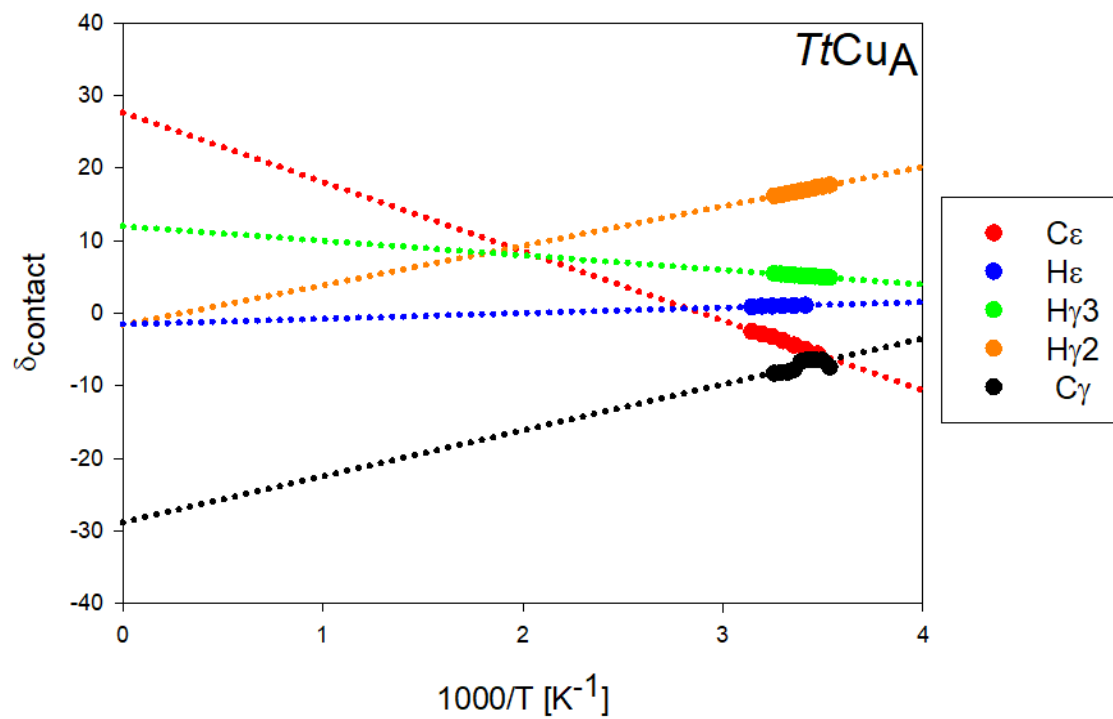


**Figure S1.** Temperature dependence of the contact shift of nuclei assigned to Met160 in *TtCu<sub>A</sub>*.

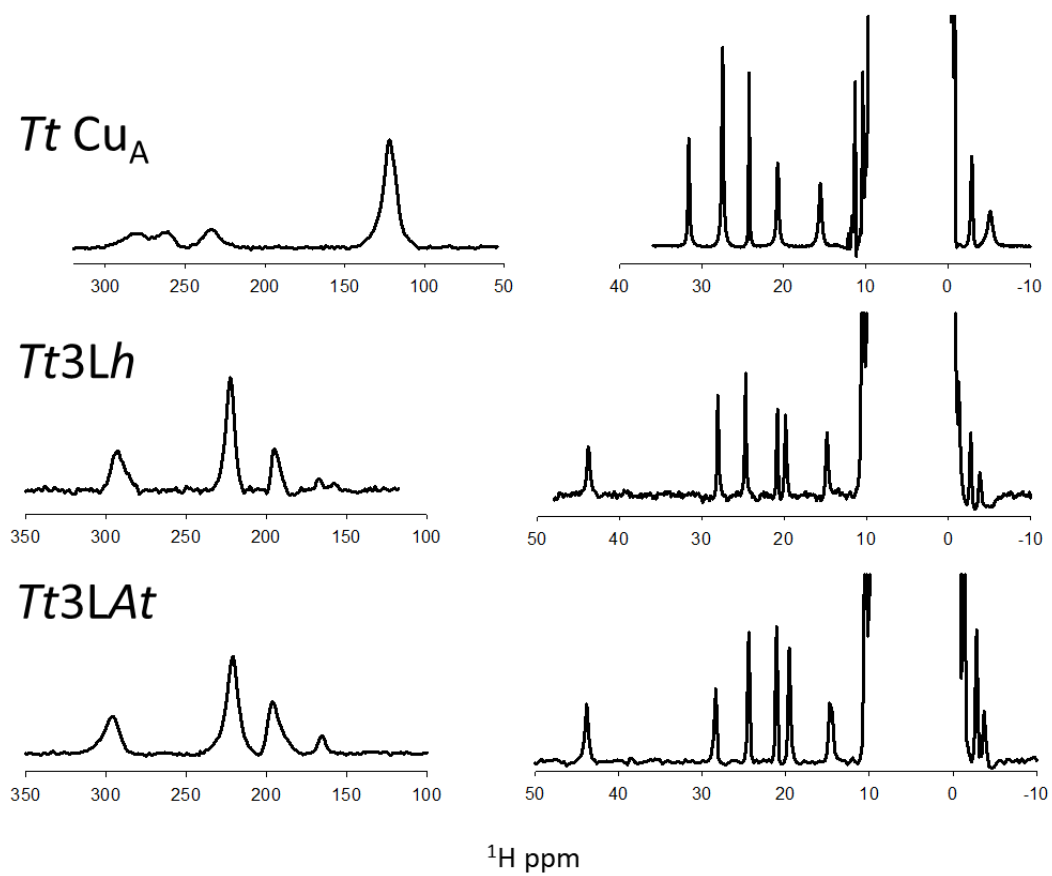


**Figure S2.**  $^1\text{H}$  NMR spectra of non-labeled wild-type  $Tt\text{Cu}_A$  and the variants  $Tt3Lh$  and  $Tt3LA$ . All spectra were recorded in phosphate buffer, 50mM, pH 6.0.

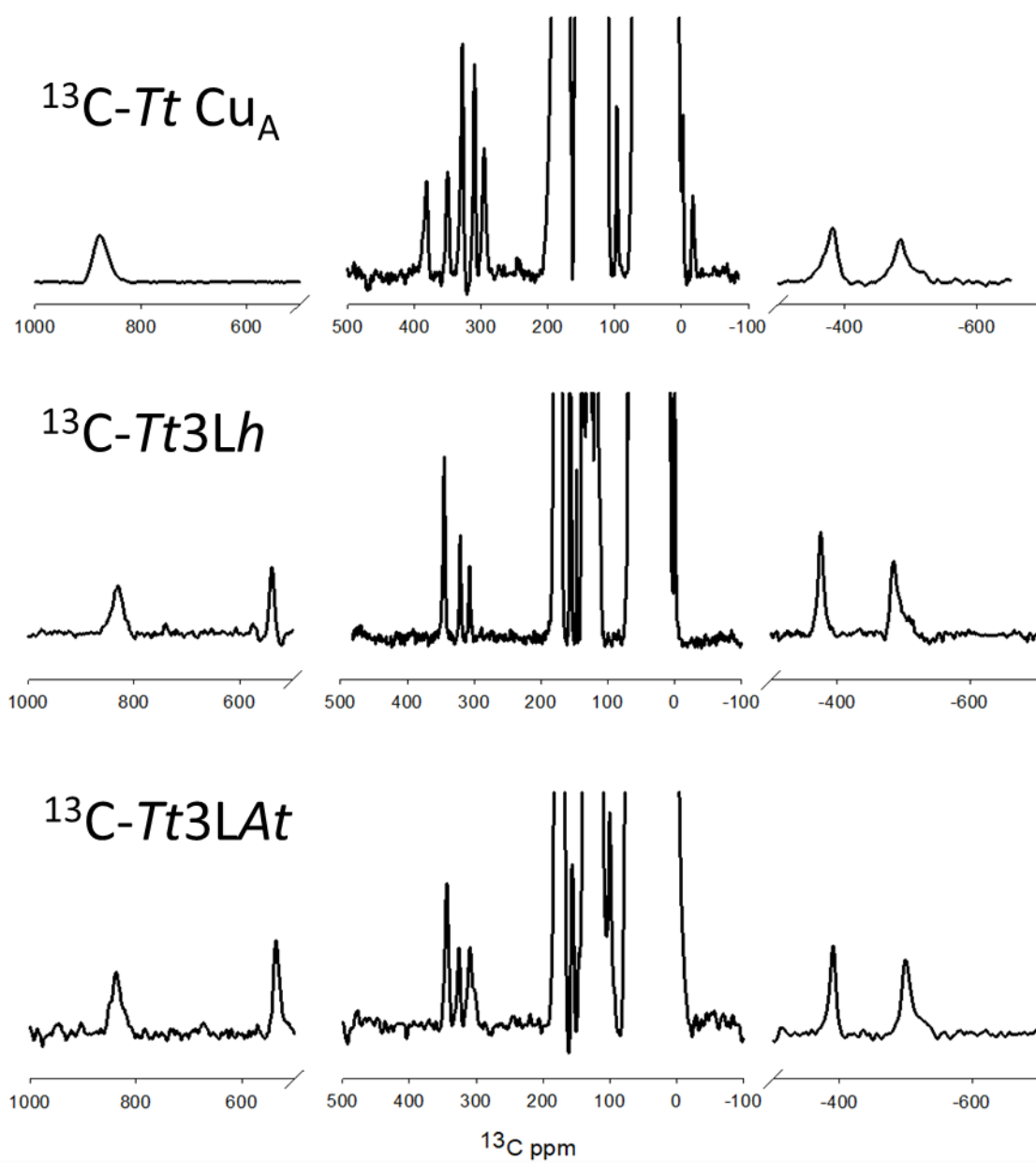


**Figure S3.**  $^{13}\text{C}$  NMR spectra of wild-type *TtCu<sub>A</sub>* and the mutant proteins *Tt3Lh* and *Tt3LAT*. All spectra were recorded in phosphate buffer, 50mM, pH 6.0.

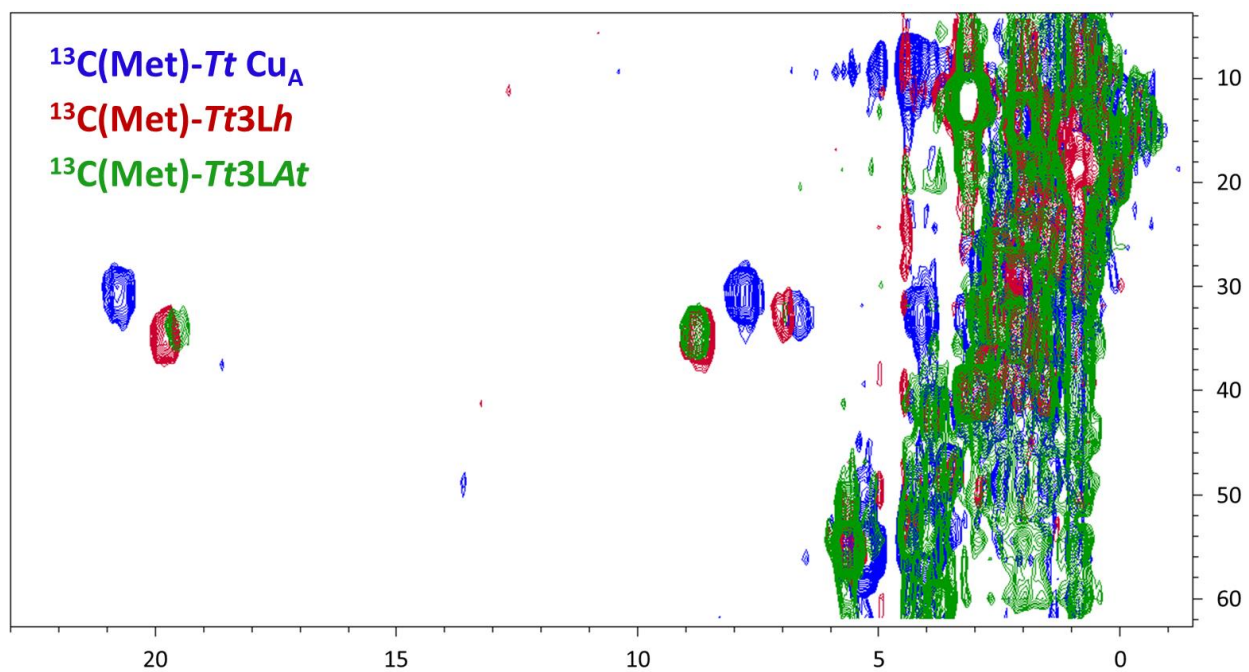


**Figure S4.** <sup>1</sup>H, <sup>13</sup>C HMQC spectra of <sup>13</sup>C-Met labeled samples of the different Cu<sub>A</sub> variants: *TtCu<sub>A</sub>* (blue), *Tt3Lh* (red) and *Tt3LAT* (green). All spectra were recorded in phosphate buffer, 50mM, pH 6.0.

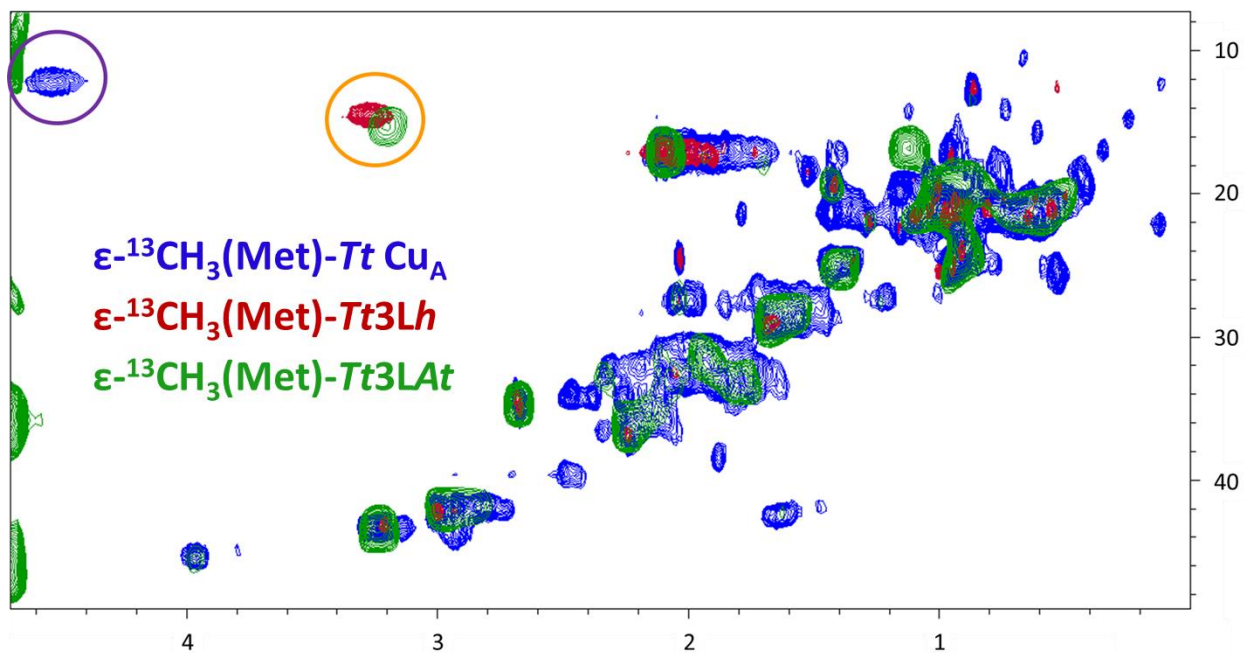


**Figure S5.**  $^1\text{H}$ ,  $^{13}\text{C}$  HMQC spectra of  $\epsilon$ - $^{13}\text{CH}_3$  labeled samples of the different Cu<sub>A</sub> variants: *Tt*Cu<sub>A</sub> (blue), *Tt3Lh* (red) and *Tt3LAt* (green). The purple and orange circles indicate the position of the  $\epsilon$ -CH<sub>3</sub>-Met on *Tt*Cu<sub>A</sub> and the chimera variants, respectively. All spectra were recorded in phosphate buffer, 50mM, pH 6.0.

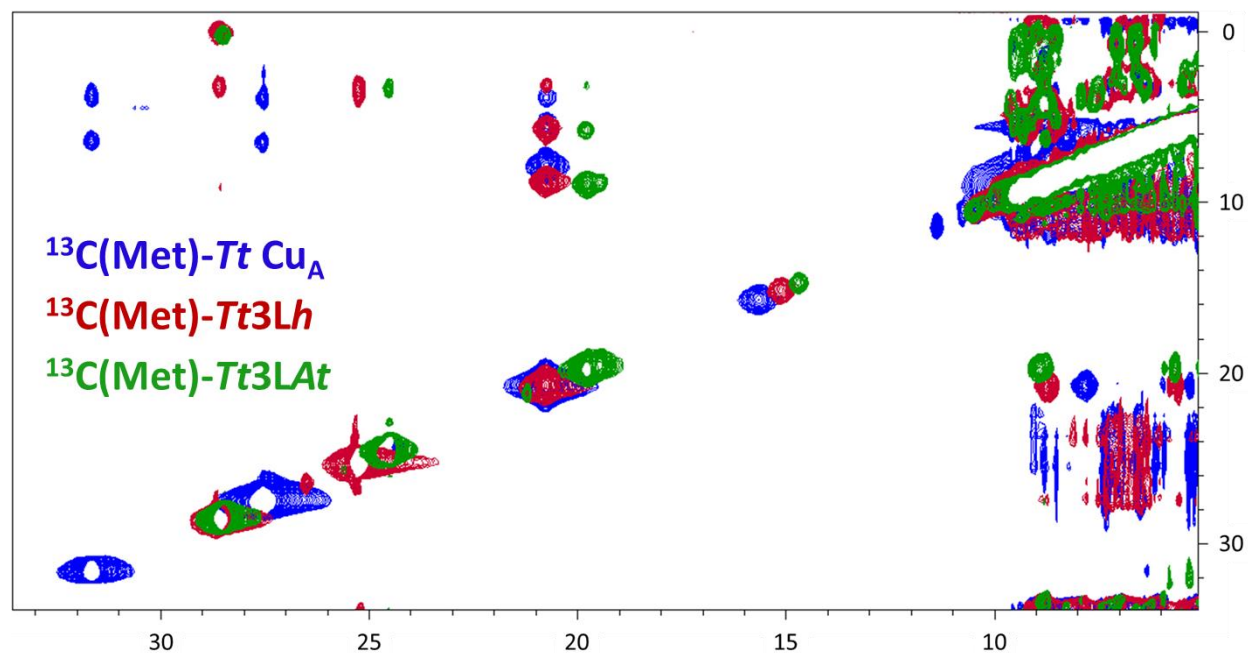


**Figure S6.**  $^1\text{H}\text{-}^1\text{H}$  NOESY experiments for all three  $\text{Cu}_A$  variants recorded with 20 ms mixing time. Colors correspond to *TtCu<sub>A</sub>* (blue), *Tt3Lh* (red) and *Tt3LAt* (green). All spectra were recorded in phosphate buffer, 50mM, pH 6.0.

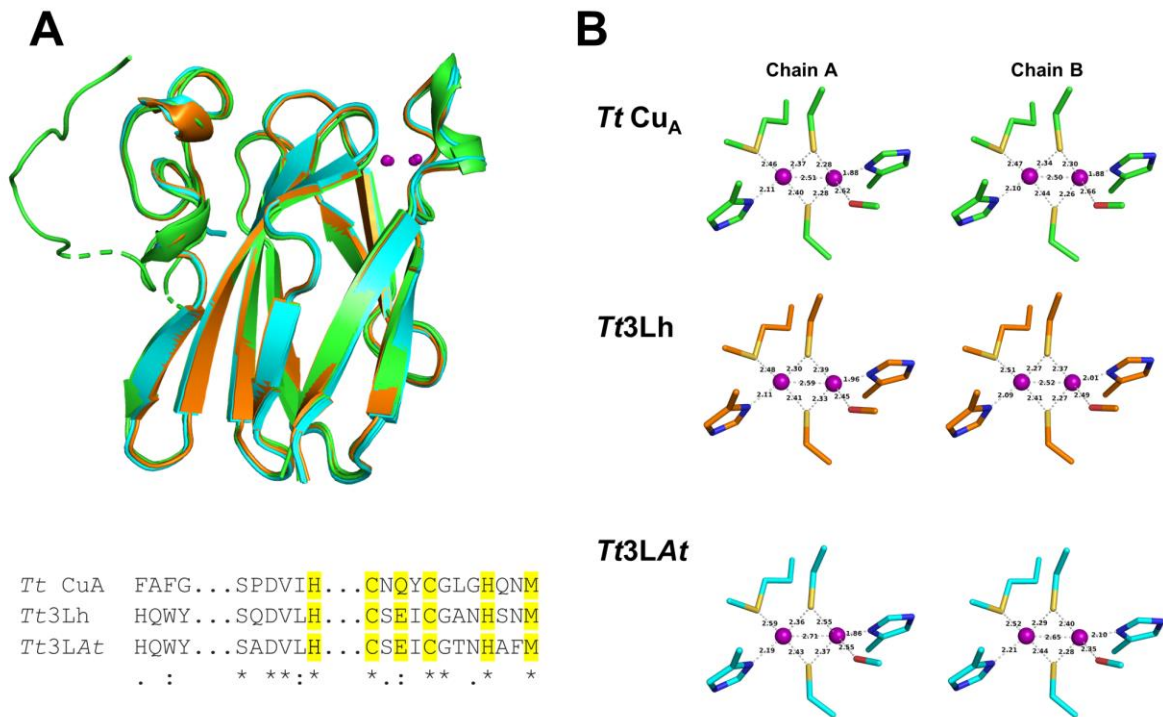


**Figure S7.** (A) Overall structure of the two chimeric proteins overlapped with wild type  $\text{Cu}_A$ . *Tt Cu<sub>A</sub>* is indicated in green, *Tt3Lh* in orange, and *Tt3LAt* in cyan. Below the structures, the sequence alignment of the three proteins in the replaced loops is shown. Metal ligands are highlighted in yellow in the sequences. (B) Metal-ligand and metal-metal distances in the  $\text{Cu}_A$  sites in all three variants. Distances corresponding to the two molecules in the asymmetric subunits are indicated.

**Table S1.** Calculated (QM) atomic spin densities and atomic electron density contributions to molecular orbitals for *TtCu<sub>A</sub>*.

Nucleus	$\delta_{\text{con}}$	Spin density	$\sigma_u^*$	$\pi_u$
Copper ions				
Cu <sub>M</sub>		0.20507	0.14	0.13
Cu <sub>O</sub>		0.2557715	0.12	0.06
His 114				
C $\gamma$	196.35	-0.00086		
C $\delta$ 2	266.41	0.00068		
C $\epsilon$ 1		-0.00193		
N $\delta$ 1		-0.00006		
N $\epsilon$ 2	74.03	0.01486	0.01	0.01
H $\delta$ 2	21.1	0.00018		
H $\epsilon$ 1		0.00037		
H $\epsilon$ 2	4.22	0.00023		
Cys 149				
S $\gamma$		0.22248	0.26	0.30
C $\alpha$	233.7	0.00108		
C $\beta$	-409.84	-0.01009	0.01	0.01
H $\alpha$	-6.25	-0.00014		
H $\beta$ 2	259.44	0.00655	0.01	0.01
H $\beta$ 3	232.45	0.00387		
Cys 153				
S $\gamma$		0.24574	0.25	0.21
C $\alpha$	824.49	0.00530	0.01	
C $\beta$	-509.99	-0.01063		
H $\alpha$	22.32	0.00033		
H $\beta$ 2	280.32	0.006	0.01	0.01
H $\beta$ 3	108.06	-0.00005	0.01	
His 157				
C $\gamma$	177	-0.00068		
C $\delta$ 2	335.35	0.00128		
C $\epsilon$ 1	-104.42	-0.00355		
N $\delta$ 1		0.0004		
N $\epsilon$ 2		0.03536	0.02	
H $\delta$ 2	24.75	0.00044		
H $\epsilon$ 1	19.3	0.00059		
H $\epsilon$ 2		0.00042		
Met 160				
S $\delta$		0.01583	0.055	0.09
C $\alpha$		-0.00002		
C $\beta$	0	0.00003		
C $\gamma$	-7	0.00007		
C $\epsilon$	-12.43	-0.00088		
H $\alpha$		0.0		
H $\beta$ 2	1.21	0.0		
H $\beta$ 3	1.05	-0.00006		
H $\gamma$ 2	16.71	0.00132		
H $\gamma$ 3	5.31	-0.00011		
H $\epsilon$	3.46	0.00024		

**Table S2.** QM subsystems used in the QM/MM simulations of *Tt* Cu<sub>A</sub>.

<b><i>Tt</i> Cu<sub>A</sub> QM residues</b>	<b>QM section</b>
HIS114	imidazole ring
CYS149	S, C $\alpha$ , C $\beta$ and corresponding H atoms
ASN150	carbonyl
GLN151	Complete aminoacid
TYR152	Complete aminoacid
CYS153	Complete aminoacid
HIS157	imidazole ring
ASN159	carbonyl
MET160	Complete aminoacid
PHE161	Complete aminoacid

**Table S3.** Observed chemical shifts ( $\delta_{\text{obs}}$ ) for the paramagnetically shifted signals on each of the analyzed Cu<sub>A</sub> variants, indicating the contribution of the diamagnetic ( $\delta_{\text{dia}}$ ), pseudocontact ( $\delta_{\text{pc}}$ ) and contact ( $\delta_{\text{con}}$ ) shifts.

Nucleus	<i>TtCu<sub>A</sub></i>				<i>Tt3Lh</i>				<i>Tt3LAt</i>			
	$\delta_{\text{obs}}$	$\delta_{\text{dia}}$	$\delta_{\text{pc}}$	$\delta_{\text{con}}$	$\delta_{\text{obs}}$	$\delta_{\text{dia}}$	$\delta_{\text{pc}}$	$\delta_{\text{con}}$	$\delta_{\text{obs}}$	$\delta_{\text{dia}}$	$\delta_{\text{pc}}$	$\delta_{\text{con}}$
His 114												
CY	331.2	135.5	-0.65	196.35	321.00	135.5 <sup>†</sup>	-0.41	185.91	309	135.5 <sup>†</sup>	-0.53	174.03
Cδ2	386.2	120.2	-0.41	266.41	306.00	120.2 <sup>†</sup>	-0.33	186.13				
Hδ2	27.46	6.66	-0.24	21.1	28.01	6.66 <sup>†</sup>	-0.17	21.58	28.5	6.76	-0.18	21.92
He2	15.5	11.78	-0.5	4.22	20.81	11.78 <sup>†</sup>	-0.47	9.5	21.1	11.78 <sup>†</sup>	-0.52	9.84
Ne2	239.7	165	-0.67	74.03	240.00	165.0 <sup>†</sup>	-0.62	75.62	237	165 <sup>†</sup>	-0.68	72.68
Gly 115												
NH	-5.2	10.1	-0.4	-14.9	-3.82	10.1	-1.05	-12.87	-3.71	9.7	-0.39	-13.02
Cys 149												
Cα	294.6	59.9	-1	233.7	539.0	59.9	-1.01	480.11	535	60.14	-1.08	475.8
Cβ	-379	32.3	-1.46	-409.84	-390.0	32.3	-1.02	-421.28	-390	32.42	-1.27	-421.15
Hα	-2.9	4.41	-1.06	-6.25	-2.67	4.41	-1.16	-5.92	-2.79	4.3	-1.17	-5.92
Hβ2	262	3.32	-0.76	259.44	293.3	3.32	0.71	289.27	295	3.2	0.15	291.65
Hβ3	237	3.05	1.5	232.45	222.3	3.05	1.53	217.72	219	3.2	1.45	214.35
Cys 153												
Cα	881	56.5	0.01	824.49	832.0	56.5	-0.17	775.67	837	58.1	-0.16	779.06
Cβ	-475	34.5	0.49	-509.99	-500.0	34.5	1.24	-535.74	-500.0	34.1	1.05	-535.15
Hα	27.55	4.54	0.64	22.32	43.72	4.54	0.49	38.69	43.8	5.0	0.48	38.32
Hβ2	283	3.08	-0.43	280.32	222.0	3.08	0.62	218.3	194	3.0	0.34	190.66
Hβ3	117	2.89	6.05	108.06	167.6	2.89	8.8	155.91	164	3.0	8.47	152.53
His 157												
CY	312.2	136.5	-1.33	177	321.0	136.5 <sup>†</sup>	-1.35	185.85	325	136.5 <sup>†</sup>	-1.34	189.84
Cδ2	353.6	119	-0.75	335.35	521.0	119.0 <sup>†</sup>	-0.73	402.73	343	119.0 <sup>†</sup>	-0.72	224.72
Cε1	33.9	140.6	-2.28	-104.42	123.0	140.6 <sup>†</sup>	-1.98	-15.62				
Hδ2	31.6	7.31	-0.46	24.75	24.7	7.31 <sup>†</sup>	-0.46	17.85	24.5	7.3	-0.46	17.66
He1	24.2	7.38	-2.48	19.3	14.75	7.38 <sup>†</sup>	-2.07	9.44	14.62	7.38 <sup>†</sup>	-1.84	9.08
Met 160												
Cβ	32.93	30.1	2.83	0	32.9	29.8	3.0	0.1	33	29.9	3.47	-0.37
CY	31.3	36.4	1.9	-7	35.5	36.4 <sup>†</sup>	1.92	-2.82	34	36.4 <sup>†</sup>	2.24	-4.64
Cε	12.5	25.8	-0.87	-12.43	14.5	25.8 <sup>†</sup>	-0.99	-10.4	12.2	25.8 <sup>†</sup>	-0.92	-12.68
Hβ2		2.64	2.82	1.21		2.72	4.3	-0.12		2.64 <sup>†</sup>	1.1	3.06
Hβ3	6.67*	1.41	4.21	1.05	6.9*	1.6	4.69	0.61	6.8*	1.14 <sup>†</sup>	3.44	2.22
HY2	20.73	2.52	1.55	16.71	19.8	2.52 <sup>†</sup>	1.44	15.88	19.54	1.4	1.74	16.4
HY3	7.8	1.56	0.93	5.31	8.76	1.56 <sup>†</sup>	0.97	6.23	8.7	2.54	1.15	5.01
He	4.54	1.91	-0.83	3.46	3.26	1.91 <sup>†</sup>	-0.95	2.3	3.2	1.8	-0.93	2.33

\*Observed chemical shift for one of the geminal protons. Geminal proton lies among the diamagnetic region and cannot be resolved.

<sup>†</sup> Diamagnetic Chemical shift based on the assignment of *TtCu<sub>A</sub>* (BMRB entry 5819)

**Table S4.** Data collection and refinement statistics

	<b><i>Tt3LA</i>t</b> (PDB ID 6PTT)	<b><i>Tt3L</i>h</b> (PDB ID 6PTY)
<b>Data collection</b>		
Wavelength (Å)	1.367875	1.367875
Space group	P2 <sub>1</sub> 2 <sub>1</sub> 2 <sub>1</sub>	P2 <sub>1</sub> 2 <sub>1</sub> 2 <sub>1</sub>
Cell dimensions		
<i>a</i> , <i>b</i> , <i>c</i> (Å)	51.33, 73.73, 79.14	51.63, 70.96, 77.42
$\alpha$ , $\beta$ , $\gamma$ (°)	90.00, 90.00, 90.00	90.00, 90.00, 90.00
Resolution (Å)	43.07 - 1.84 (1.88 - 1.84) <sup>a</sup>	42.95 - 1.98 (2.03 - 1.98)
<i>R</i> <sub>merge</sub>	0.078 (0.438)	0.058 (0.309)
<i>I</i> / $\sigma$ <i>I</i>	16.1 (3.0)	17.5 (3.0)
CC(1/2)	0.990 (0.896)	0.998 (0.981)
Completeness (%)	98.2 (99.5)	99.1 (98.5)
Redundancy	4.1 (4.1)	5.0 (4.8)
<b>Refinement</b>		
Resolution (Å)	43.07 - 1.84 (1.91 - 1.84)	42.95 - 1.98 (2.08 - 1.98)
No. reflections	26,058 (2,556)	20,141 (2,749)
<i>R</i> <sub>work</sub> / <i>R</i> <sub>free</sub>	16.97/21.37	19.82/23.83
No. atoms		
Protein	1,896	1,894
Cu	4	4
Sulfate	-	5
Glycerol	-	6
Water	250	229
<i>B</i> -factors		
Protein	26.29	28.76
Cu	30.39	43.09
Sulfate	-	50.80
Glycerol	-	29.79
Water	38.80	37.78
R.m.s. deviations		
Bond lengths (Å)	0.02	0.004
Bond angles (°)	1.19	0.68

\*One protein crystal was employed for structure determination. Values in parentheses are for highest-resolution shell.

## REFERENCES

- (1) O'Grady, C.; Rempel, B. L.; Sokaribo, A.; Nokhrin, S.; Dmitriev, O. Y. One-step amino acid selective isotope labeling of proteins in prototrophic *Escherichia coli* strains. *Analytical Biochemistry* **2012**, *426*, 126.
- (2) Leguto, A. J.; Smith, M. A.; Morgada, M. N.; Zitare, U. A.; Murgida, D. H.; Lancaster, K. M.; Vila, A. J. Dramatic Electronic Perturbations of CuA Centers via Subtle Geometric Changes. *J Am Chem Soc* **2019**, *141*, 1373.
- (3) Kabsch, W. Integration, scaling, space-group assignment and post-refinement. *Acta Crystallographica Section D Biological Crystallography* **2010**, *66*, 133.
- (4) Morgada, M. N.; Abriata, L. A.; Zitare, U.; Alvarez-Paggi, D.; Murgida, D. H.; Vila, A. J. Control of the electronic ground state on an electron-transfer copper site by second-sphere perturbations. *Angew Chem Int Ed Engl* **2014**, *53*, 6188.
- (5) Abriata, L. A.; Ledesma, G. N.; Pierattelli, R.; Vila, A. J. Electronic structure of the ground and excited states of the Cu(A) site by NMR spectroscopy. *J Am Chem Soc* **2009**, *131*, 1939.
- (6) Neese, F.; Zumft, W. G.; Antholine, W. E.; Kroneck, P. M. H. The Purple Mixed-Valence CuA Center in Nitrous-oxide Reductase: EPR of the Copper-63-, Copper-65-, and Both Copper-65- and [15N]Histidine-Enriched Enzyme and a Molecular Orbital Interpretation. *Journal of the American Chemical Society* **1996**, *118*, 8692.
- (7) Evans, P. R.; Murshudov, G. N. How good are my data and what is the resolution? *Acta Crystallographica Section D Biological Crystallography* **2013**, *69*, 1204.
- (8) Winn, M. D.; Ballard, C. C.; Cowtan, K. D.; Dodson, E. J.; Emsley, P.; Evans, P. R.; Keegan, R. M.; Krissinel, E. B.; Leslie, A. G. W.; McCoy, A.; McNicholas, S. J.; Murshudov, G. N.; Pannu, N. S.; Potterton, E. A.; Powell, H. R.; Read, R. J.; Vagin, A.; Wilson, K. S. Overview of the CCP4 suite and current developments. *Acta Crystallographica Section D Biological Crystallography* **2011**, *67*, 235.
- (9) McCoy, A. J.; Grosse-Kunstleve, R. W.; Adams, P. D.; Winn, M. D.; Storoni, L. C.; Read, R. J. Phaser crystallographic software. *Journal of Applied Crystallography* **2007**, *40*, 658.
- (10) Williams, P. A.; Blackburn, N. J.; Sanders, D.; Bellamy, H.; Stura, E. A.; Fee, J. A.; McRee, D. E. The CuA domain of *Thermus thermophilus* ba3-type cytochrome c oxidase at 1.6 Å resolution. *Nat Struct Biol* **1999**, *6*, 509.
- (11) Emsley, P.; Lohkamp, B.; Scott, W. G.; Cowtan, K. Features and development of Coot. *Acta Crystallographica Section D Biological Crystallography* **2010**, *66*, 486.
- (12) Afonine, P. V.; Grosse-Kunstleve, R. W.; Echols, N.; Headd, J. J.; Moriarty, N. W.; Mustyakimov, M.; Terwilliger, T. C.; Urzhumtsev, A.; Zwart, P. H.; Adams, P. D. Towards automated crystallographic structure refinement with phenix.refine. *Acta Crystallographica Section D Biological Crystallography* **2012**, *68*, 352.
- (13) Adams, P. D.; Afonine, P. V.; Bunkóczi, G.; Chen, V. B.; Davis, I. W.; Echols, N.; Headd, J. J.; Hung, L.-W.; Kapral, G. J.; Grosse-Kunstleve, R. W.; McCoy, A. J.; Moriarty, N. W.; Oeffner, R.; Read, R. J.; Richardson, D. C.; Richardson, J. S.; Terwilliger, T. C.; Zwart, P. H. PHENIX: a comprehensive Python-based system for macromolecular structure solution. *Acta Crystallographica Section D Biological Crystallography* **2010**, *66*, 213.
- (14) Williams, C. J.; Headd, J. J.; Moriarty, N. W.; Prisant, M. G.; Videau, L. L.; Deis, L. N.; Verma, V.; Keedy, D. A.; Hintze, B. J.; Chen, V. B.; Jain, S.; Lewis, S. M.; Arendall, W. B.; Snoeyink, J.; Adams, P. D.; Lovell, S. C.; Richardson, J. S.; Richardson, D. C. MolProbity: More and better reference data for improved all-atom structure validation. *Protein Science* **2018**, *27*, 293.
- (15) D.A. Case, R. M. B., D.S. Cerutti, T.E. Cheatham, III, T.A. Darden, R.E. Duke, T.J. Giese, H. Gohlke, A.W. Goetz, N. Homeyer, S. Izadi, P. Janowski, J. Kaus, A. Kovalenko, T.S. Lee, S. LeGrand, P.

Li, C.Lin, T. Luchko, R. Luo, B. Madej, D. Mermelstein, K.M. Merz, G. Monard, H. Nguyen, H.T. Nguyen, I.Omelyan, A. Onufriev, D.R. Roe, A. Roitberg, C. Sagui, C.L. Simmerling, W.M. Botello-Smith, J. Swails, R.C. Walker, J. Wang, R.M. Wolf, X. Wu, L. Xiao and P.A. Kollman *AMBER 2016* San Francisco, 2016.

(16) Salomon-Ferrer, R.; Götz, A. W.; Poole, D.; Le Grand, S.; Walker, R. C. Routine Microsecond Molecular Dynamics Simulations with AMBER on GPUs. 2. Explicit Solvent Particle Mesh Ewald. *Journal of Chemical Theory and Computation* **2013**, *9*, 3878.

(17) Le Grand, S.; Götz, A. W.; Walker, R. C. SPFP: Speed without compromise—A mixed precision model for GPU accelerated molecular dynamics simulations. *Computer Physics Communications* **2013**, *184*, 374.

(18) Li, P.; Merz, K. M. MCPB.py: A Python Based Metal Center Parameter Builder. *Journal of Chemical Information and Modeling* **2016**, *56*, 599.

(19) Izquierdo, J.; Vega, A.; Balbás, L. C.; Sánchez-Portal, D.; Junquera, J.; Artacho, E.; Soler, J. M.; Ordejón, P. Systematicab initiostudy of the electronic and magnetic properties of different pure and mixed iron systems. *Physical Review B* **2000**, *61*, 13639.

(20) Crespo, A.; Scherlis, D. A.; Martí, M. A.; Ordejón, P.; Roitberg, A. E.; Estrin, D. A. A DFT-Based QM-MM Approach Designed for the Treatment of Large Molecular Systems: Application to Chorismate Mutase. *The Journal of Physical Chemistry B* **2003**, *107*, 13728.

(21) Perdew, J. P.; Burke, K.; Ernzerhof, M. Generalized Gradient Approximation Made Simple. *Physical Review Letters* **1996**, *77*, 3865.

(22) M. J. Frisch, G. W. T., H. B. Schlegel, G. E. Scuseria, M. A. Robb, J. R. Cheeseman, G. Scalmani, V. Barone, G. A. Petersson, H. Nakatsuji, X. Li, M. Caricato, A. Marenich, J. Bloino, B. G. Janesko, R. Gomperts, B. Mennucci, H. P. Hratchian, J. V. Ortiz, A. F. Izmaylov, J. L. Sonnenberg, D. Williams-Young, F. Ding, F. Lipparini, F. Egidi, J. Goings, B. Peng, A. Petrone, T. Henderson, D. Ranasinghe, V. G. Zakrzewski, J. Gao, N. Rega, G. Zheng, W. Liang, M. Hada, M. Ehara, K. Toyota, R. Fukuda, J. Hasegawa, M. Ishida, T. Nakajima, Y. Honda, O. Kitao, H. Nakai, T. Vreven, K. Throssell, J. A. Montgomery, Jr., J. E. Peralta, F. Ogliaro, M. Bearpark, J. J. Heyd, E. Brothers, K. N. Kudin, V. N. Staroverov, T. Keith, R. Kobayashi, J. Normand, K. Raghavachari, A. Rendell, J. C. Burant, S. S. Iyengar, J. Tomasi, M. Cossi, J. M. Millam, M. Klene, C. Adamo, R. Cammi, J. W. Ochterski, R. L. Martin, K. Morokuma, O. Farkas, J. B. Foresman, and D. J. Fox *Gaussian 09, Revision A.02*, 2016.